Original Article | Musculoskeletal Imaging

eISSN 2005-8330
https://doi.org/10.3348/kjr.2018.0032
Korean J Radiol 2019;20(6):916-930

Korean Journal of Radiology
KJR

Simultaneous Estimation of the Fat Fraction and R_2* Via T_2*-Corrected 6-Echo Dixon Volumetric Interpolated Breath-hold Examination Imaging for Osteopenia and Osteoporosis Detection: Correlations with Sex, Age, and Menopause

Donghyun Kim, MD[1], Sung Kwan Kim, MD[1], Sun Joo Lee, MD, PhD[1], Hye Jung Choo, MD, PhD[1], Jung Won Park, MD[1], Kun Yung Kim, MD, PhD[2]

[1]Department of Radiology, Inje University College of Medicine, Busan Paik Hospital, Busan, Korea; [2]Department of Radiology, Chonbuk National University Hospital, Jeonju, Korea

Objective: To investigate the relationships of T_2*-corrected 6-echo Dixon volumetric interpolated breath-hold examination (VIBE) imaging-based fat fraction (FF) and R_2* values with bone mineral density (BMD); determine their associations with sex, age, and menopause; and evaluate the diagnostic performance of the FF and R_2* for predicting osteopenia and osteoporosis.

Materials and Methods: This study included 153 subjects who had undergone magnetic resonance (MR) imaging, including MR spectroscopy (MRS) and T_2*-corrected 6-echo Dixon VIBE imaging. The FF and R_2* were measured at the L4 vertebra. The male and female groups were divided into two subgroups according to age or menopause. Lin's concordance and Pearson's correlation coefficients, Bland-Altman 95% limits of agreement, and the area under the curve (AUC) were calculated.

Results: The correlation between the spectroscopic and 6-echo Dixon VIBE imaging-based FF values was statistically significant for both readers (p_c = 0.940 [reader 1], 0.908 [reader 2]; both p < 0.001). A small measurement bias was observed for the MRS-based FF for both readers (mean difference = -0.3% [reader 1], 0.1% [reader 2]). We found a moderate negative correlation between BMD and the FF (r = -0.411 [reader 1], -0.436 [reader 2]; both p <0.001) with younger men and premenopausal women showing higher correlations. R_2* and BMD were more significantly correlated in women than in men, and the highest correlation was observed in postmenopausal women (r = 0.626 [reader 1], 0.644 [reader 2]; both p < 0.001). For predicting osteopenia and osteoporosis, the FF had a higher AUC in men and R_2* had a higher AUC in women. The AUC for predicting osteoporosis was highest with a combination of the FF and R_2* in postmenopausal women (AUC = 0.872 [reader 1], 0.867 [reader 2]; both p < 0.001).

Conclusion: The FF and R_2* measured using T_2*-corrected 6-echo Dixon VIBE imaging can serve as predictors of osteopenia and osteoporosis. R_2* might be useful for predicting osteoporosis, especially in postmenopausal women.

Keywords: *Osteoporosis; Magnetic resonance imaging; Fat fraction; R_2*; Bone marrow*

INTRODUCTION

The Consensus Development Conference on Osteoporosis defined osteoporosis as "a systemic skeletal disease characterized by low bone mass and microarchitectural deterioration of bone tissue, with a consequent increase

Received January 11, 2018; accepted after revision January 14, 2019.
This study was supported by 2017 Inje University Busan Paik Hospital research grant.
Corresponding author: Sun Joo Lee, MD, PhD, Department of Radiology, Busan Paik Hospital, Inje University College of Medicine, 75 Bokji-ro, Busanjin-gu, Busan 47392, Korea.
• Tel: (8251) 890-6579 • Fax: (8251) 896-1085 • E-mail: sunjulee98@gmail.com

Korean Journal of Radiology
KJR

in bone fragility and susceptibility to fracture" (1). Early detection and proper management are necessary for the prevention of osteoporotic fractures and complications (2). Bone mineral density (BMD), which can be measured using dual-energy X-ray absorptiometry (DXA), is the most widely used parameter for diagnosing osteoporosis and assessing fracture risk (2, 3). Recent studies have indicated strong connections between marrow adipogenesis and osteoporosis pathophysiology. Osteoblasts and adipocytes are derived from the same progenitor cells. When the conversion of progenitor cells to adipocytes is dominant, bone formation and BMD decrease (4). Consequently, vertebral marrow fat has become a target for the diagnosis of osteoporosis. Magnetic resonance spectroscopy (MRS) is widely used as the gold standard for fat quantification (5-10), and many previous MRS studies have demonstrated a negative correlation between vertebral marrow fat content and BMD (8-12).

Various chemical shift-based water-fat separation techniques have been recently developed, and their results are consistent with those of MRS (13-15). Many confounding factors affecting fat quantification when using water-fat separation techniques have been identified (14-16). It is crucial to correct for the T_2* shortening effect caused by the presence of trabecular bone, especially for vertebral marrow fat quantification (6, 7). Multi-echo three-dimensional (3D) gradient echo imaging, which corrects for T_1 bias and the T_2* effect, allows for accurate fat fraction (FF) estimation and has the advantages of high spatial resolution and rapid acquisition (17-20). An additional advantage of this technique is that the R_2* map is provided simultaneously with fat quantification since R_2* is equivalent to $1/T_2$* (21, 22). To our knowledge, only a few studies have reported on the efficacy of R_2* as a marker for osteoporosis (22). In the English literature, correlations between the FF, R_2*, and BMD, including differences in the degree of correlation with age, have not been reported.

The purpose of our study was to investigate the relationships of T_2*-corrected 6-echo Dixon volumetric interpolated breath-hold examination (VIBE) imaging-based FF and R_2* values with BMD; determine their associations with sex, age, and menopause; and evaluate the diagnostic performance of the FF and R_2* for predicting osteopenia and osteoporosis.

MATERIALS AND METHODS

Study Population

Institutional Review Board approval was obtained and informed consent was waived. This retrospective study enrolled 228 patients who had undergone DXA and lumbar spine magnetic resonance imaging (MRI) for the evaluation of lower back pain between July and December 2016. These patients underwent MRS and T_2*-corrected 6-echo Dixon VIBE imaging. Patients who had previously undergone lumbar spinal surgery (n = 28) or had compression fractures at L4 (n = 21) or large osteophytes (n = 26) were excluded. Thus, the final study population consisted of 153 patients (69 men and 84 women; mean age, 63.2 ± 8.2 years; age range, 31–81 years). BMD was normal in 99 subjects. Osteopenia and osteoporosis were observed in 37 and 17 subjects, respectively. The men and women were divided into two subgroups according their age (≥ 50 years) and menopause status, respectively. Height and body weight data were collected from each subject's medical records. There were significant differences in age, vertebral BMD, and T-scores between men and women; however, there was no difference in body mass index. The demographic and clinical characteristics of the study population are listed in Table 1.

DXA Examination

All DXA examinations of the lumbar spine (L1–4) were performed using a Lunar Prodigy scanner (GE Medical Systems, Madison, WI, USA). The areal BMD (g/cm^2) and

Table 1. Baseline Characteristics of Study Subjects

	Males (n = 69)		Females (n = 84)		*P**
	Age < 50 Years (n = 6)	Age ≥ 50 Years (n = 63)	Premenopausal (n = 7)	Postmenopausal (n = 77)	
Age, years	41.2 (7.4)	63.5 (6.0)	49.0 (3.1)	65.9 (6.0)	0.034‡
Body mass index, kg/m^2	26.4 (3.4)	24.8 (2.6)	27.5 (3.5)	24.8 (3.3)	0.844†
L1–4 vertebral BMD (g/cm^2)	1.19 (0.17)	1.16 (0.15)	1.24 (0.25)	0.98 (0.15)	< 0.001‡
T-score	-1.2 (1.6)	0.4 (1.3)	-1.6 (1.7)	-0.7 (1.6)	< 0.001†

Data are presented as mean and standard deviations (in parenthesis). *p values were obtained in comparison between male and female groups using following methods, †Independent t test, ‡Mann-Whitney U test. BMD = bone mineral density

 https://doi.org/10.3348/kjr.2018.0032

T-scores were assessed for all enrolled patients. Normal BMD, osteopenia, and osteoporosis were defined as T-score ≥ -1.0 standard deviation (SD), -2.5 < T-score < -1.0 SD, and T-score ≤ -2.5 SD, respectively (2).

MRI Protocol

All MRI examinations were performed on a 3T MRI scanner (MAGNETOM Skyra; Siemens Healthineers, Erlangen, Germany). The mean interval between the DXA and MRI examinations was 3 days (range, 0–30 days). All images were acquired with subjects in the supine position using a standard spine array coil and an eight-channel phased array coil for the spine. Conventional MRI sequences for anatomical and morphological evaluation of the lumbar vertebrae were adopted, and the imaging parameters are summarized in Table 2.

A single-voxel high-speed T_2-corrected multi-echo (HISTO) MRS sequence was performed using a stimulated echo acquisition mode with the following parameters: repetition time = 3000 ms; echo time (TE) = 12, 24, 36, 48, and 72 ms; bandwidth = 1200 Hz; flip angle = 90°; and voxel size = 15 x 15 x 15 mm^3. The scan time was 45 seconds. A spectroscopic voxel was placed on the anterior aspect of the L4 vertebral body. An example of the water and fat spectral peaks at a specific TE and the automatically calculated FF from the HISTO scan are displayed in Figure 1A.

For water-fat separation and FF estimation, T_2*-corrected 6-echo Dixon VIBE imaging was performed. The imaging parameters are summarized in Table 2. We used a small flip angle to minimize the T_1 bias. Images were obtained at the L4 vertebral body in the sagittal plane. For the calculation of the FF map, multi-peak fat spectral modeling was used for more precise T_2* correction. The FF and R_2* maps were automatically generated from the T_2*-corrected 6-echo Dixon VIBE imaging series.

Data Analysis

Two experienced musculoskeletal radiologists who were blinded to the DXA results and MRS-based FF information performed all measurements independently and estimated the FF and R_2*. These parameters were calculated from automatically reconstructed FF and R_2* maps loaded onto an imaging workstation (Syngo software version B17; Siemens Healthineers, Forchheim, Germany). Regions of interest (ROIs) were manually drawn on the L4 vertebral body in mid-sagittal view using a fat-only image. These ROIs were directly copied onto the FF and R_2* maps. The ROIs were located at least 2 mm from the endplate, and the basivertebral plexus and focal fat deposition were excluded (Fig. 1B). ROI size varied according to the area of the spine. The mean ROI sizes were 424 ± 82 mm^2 for reader 1 and 420 ± 50 mm^2 for reader 2.

Statistical Analysis

All continuous variables were assessed for normality using the Shapiro-Wilk test and are presented as mean ± SD. We used the independent *t* test or Mann-Whitney U test to assess differences between men and women.

The interobserver agreement between the FF and R_2* measurements was analyzed using the intraclass correlation coefficient (ICC) with a two-way random effects model of absolute agreement. The interobserver agreement was interpreted as follows: < 0.50, poor; 0.50–0.75, moderate; 0.75–0.90, good; and > 0.90, excellent (23).

To assess the consistency between the FF values obtained via T_2*-corrected 6-echo Dixon VIBE imaging and MRS, Lin's

Table 2. Summary of MRI Parameters for Fat Quantification

Sequence Parameters	Sagittal T1-Weighted TSE Image	Sagittal T2-Weighted TSE Image	T_2*-Corrected Six-Echo 3D VIBE GRE Image
Repetition time (ms)	619	3900	10.1
TE (ms)	9.5	106	1.45 (TE 1), ΔTE = 1.37
Echo train length	2	21	6
Matrix size	448 x 314	512 x 358	256 x 256
Field of view (cm)	35 x 35	35 x 35	30 x 30
Slice thickness (mm)	3.0	3.0	3.0
Intersection gap (mm)	0.3	0.3	No gap
Flip angle (°)	150	150	4
Number of excitations	3	1	1
Scan time	2 min 50 sec	2 min 18 sec	53 sec

GRE = gradient echo, TE = echo time, TSE = turbo spin echo, VIBE = volumetric interpolated breath-hold examination

https://doi.org/10.3348/kjr.2018.0032

Korean Journal of Radiology
KJR

concordance correlation coefficient (p_c) and Bland-Altman plot with a 95% confidence interval (CI) were used. The p_c was classified as follows: > 0.99, almost perfect; 0.95–0.99, substantial; 0.90–0.95, moderate; and < 0.90, poor (24). Pearson's correlation analysis was performed to analyze the correlation between the FF and BMD in all patients and each subgroup as well as the correlation between R_2* and BMD. Pearson's correlation coefficient (*r*) was interpreted as follows: *r* = ± 1.0, perfect; ± 0.60–0.80, strong; ± 0.40–0.60, moderate; ± 0.20–0.40, weak; and 0, no correlation (25). The scatterplots are shown in Figures 2 and 3. To determine the diagnostic performance of the parameters for predicting osteopenia and osteoporosis, receiver operating characteristic (ROC) curves were constructed, and the areas under the curve (AUCs) were calculated by each reader. Using ROC curves, we compared a logistic regression model combining the FF and R_2* with those including the FF or R_2* alone. The AUCs were compared using the DeLong test and interpreted as follows: 0.90–1.0, excellent; 0.80–0.90, good; 0.70–0.80, fair; 0.60–0.70, poor; and 0.50–0.60, failed (26). A *p* value < 0.05 was considered statistically significant. All statistical analyses were performed using SPSS 22.0 (IBM Corp., Armonk, NY, USA) and MedCalc version 17.9.7 (MedCalc Software, Ostend, Belgium).

RESULTS

Interobserver Agreement

The interobserver agreement between the two radiologists for the FF and R_2* measurements was excellent. The ICC values for the FF and R_2* were 0.955 (95% CI, 0.938–0.967) and 0.953 (95% CI, 0.936–0.966), respectively.

Consistency between the FF Values Obtained Via T_2*-Corrected 6-Echo Dixon VIBE Imaging and MRS

Lin's p_c showed a moderate correlation between the

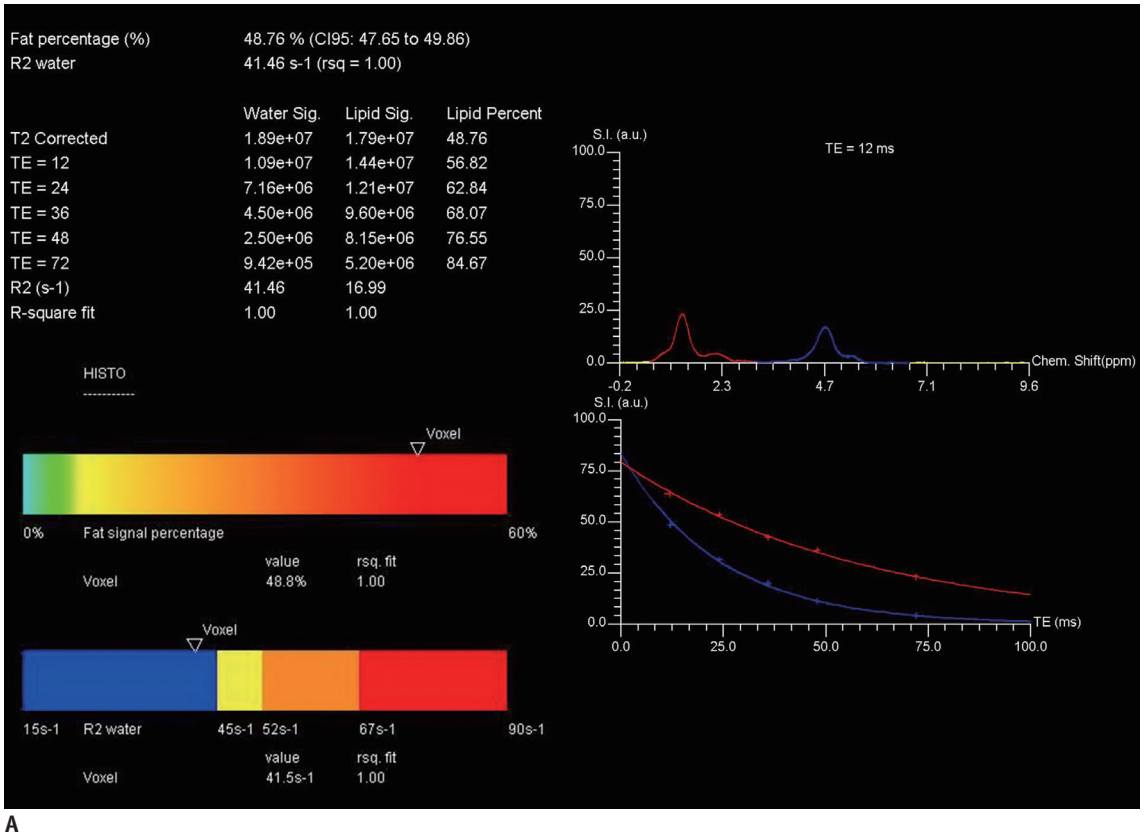

A

Fig. 1. 71-year-old female subject with lower back pain.
Screen-captured images of single-voxel T_2-corrected multi-echo MRS **(A)** and T_2*-corrected 6-echo Dixon VIBE imaging **(B)**. **A.** FF of single-voxel HISTO MRS scan. Each water and fat integral at five echoes (TE = 12, 24, 36, 48, and 72 ms; top left) with estimated FF of 48.8% (bottom left). Water and fat spectral peaks at TE of 12 ms are shown. Red curve represents 1.3-ppm fat spectrum, and blue curve represents 4.7-ppm water spectrum (top right). Image on right shows T_2 exponential decay curve. Chem. = chemical, CI = confidence interval, FF = fat fraction, HISTO = high-speed T_2-corrected multi-echo, MRS = magnetic resonance spectroscopy, rsq = r-squared, S.I. (a.u.) = signal intensity (arbitrary units), TE = echo time, VIBE = volumetric interpolated breath-hold examination

 https://doi.org/10.3348/kjr.2018.0032

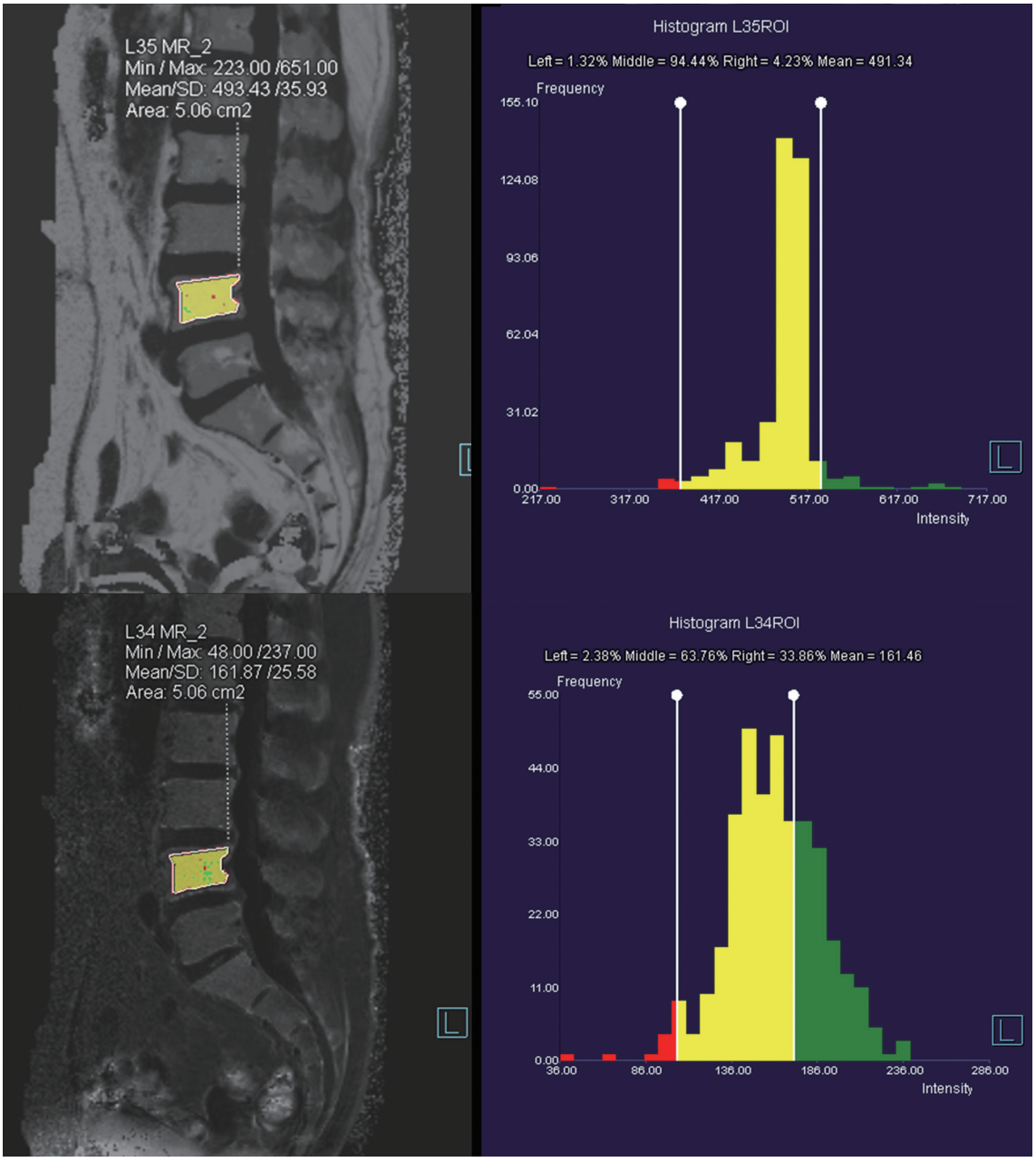

B

Fig. 1. 71-year-old female subject with lower back pain.
Screen-captured images of single-voxel T_2-corrected multi-echo MRS **(A)** and T_2*-corrected 6-echo Dixon VIBE imaging **(B)**. **B.** Measurement of FF and R_2* at MR imaging workstation (Syngo software; Siemens Healthineers). Free-drawn polygonal ROIs was located at least 2 mm from endplate and excluded basivertebral plexus. ROIs were drawn on fat-only images (top left) and directly copied onto R_2* map (bottom right). FF and R_2* are displayed as histograms (right). FF = fat fraction, MR = magnetic resonance, MRS = magnetic resonance spectroscopy, ROI = region of interest, SD = standard deviation, VIBE = volumetric interpolated breath-hold examination

FF values obtained via T_2*-corrected 6-echo Dixon VIBE imaging and MRS for readers 1 and 2 (p_c = 0.940 [reader 1], 0.908 [reader 2]; both $p < 0.001$) (Fig. 2). Figure 4 shows the mean measurement bias with limits of agreement for the FF derived from T_2*-corrected 6-echo Dixon VIBE imaging relative to the FF measured with MRS. The mean measurement biases were -0.3% (95% limits of agreement, -6.4–5.8%) for reader 1% and 0.1% (95% limits of agreement, -4.8–5.0%) for reader 2.

Correlations between BMD and the FF or R_2*

A moderate negative correlation was observed between

https://doi.org/10.3348/kjr.2018.0032

Korean Journal of Radiology
KJR

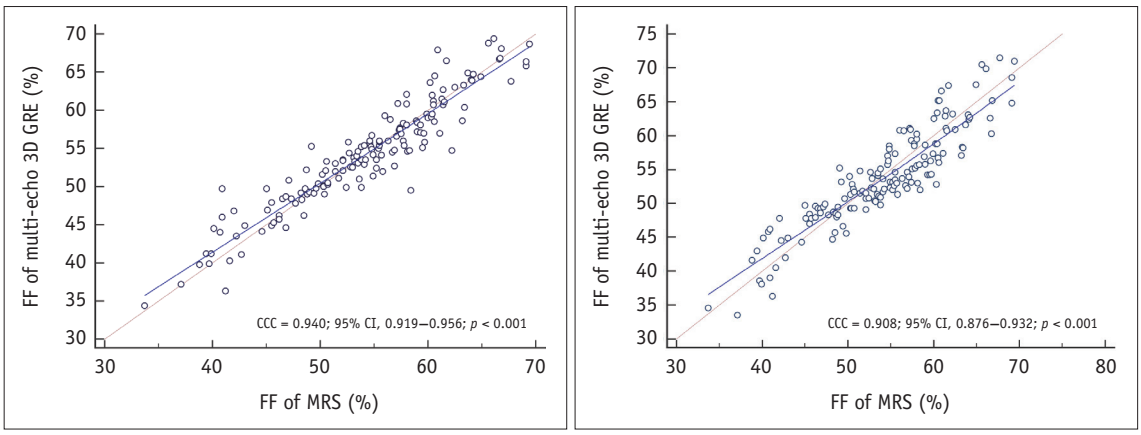

Fig. 2. Comparison between FF values measured with T_2*-corrected 6-echo Dixon VIBE imaging and MRS at L4 vertebra.
p_c for assessment of agreement between FF values measured via MRS and T_2*-corrected 6-echo Dixon VIBE imaging (reader 1, **A**; reader 2, **B**). Correlation between spectroscopic and T_2*-corrected 6-echo Dixon VIBE-based FF values was statistically significant for readers 1 and 2 (both p < 0.001). p_c values for readers 1 and 2 were 0.940 and 0.908, respectively. CCC = concordance correlation coefficient, GRE = gradient echo, 3D = three-dimensional

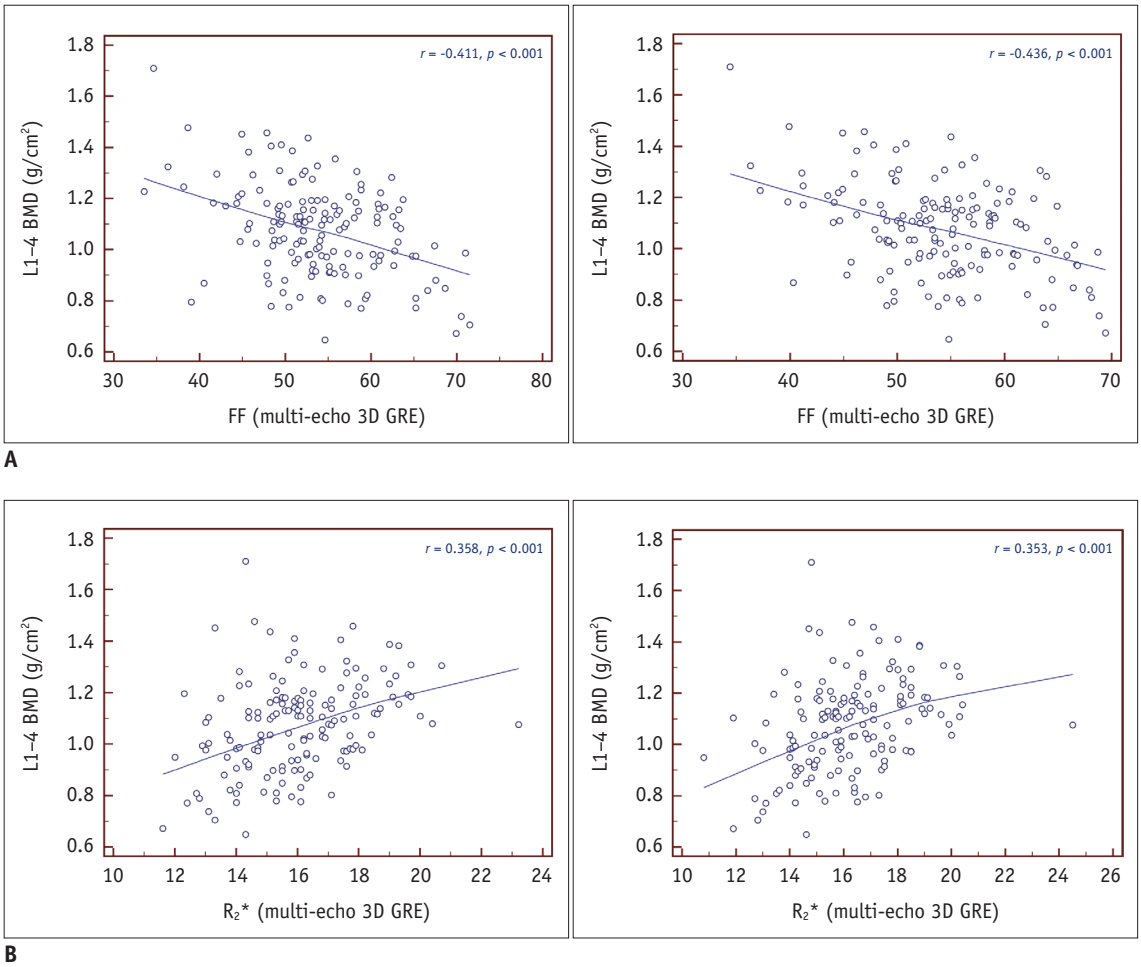

Fig. 3. Correlations between BMD and FF or R2*.
A. Scatterplot displaying correlation between FF obtained via T_2*-corrected 6-echo Dixon VIBE imaging and areal BMD (g/cm^2; reader 1, **A**-left; reader 2, **A**-right). Moderate negative correlation between FF and areal BMD was found (r = -0.411 [reader 1], -0.436 [reader 2]; both p < 0.001). **B.** Scatterplot displaying correlation between R_2*and areal BMD (g/cm^2; reader 1, **B**-left; reader 2, **B**-right). Weak positive correlation between R_2*and areal BMD was found (r = 0.358 [reader 1], 0.353 [reader 2]; both p <0.001). BMD = bone mineral density

https://doi.org/10.3348/kjr.2018.0032

the FF and areal BMD (g/cm^2) for both readers (r = -0.411 [reader 1], -0.436 [reader 2]; both p < 0.001) (Fig. 3A). There was no significant difference in the degree of correlation between men and women, and the most negative correlation was observed in younger men for both readers (r = -0.831 [reader 1], -0.801 [reader 2]; p = 0.041, 0.056) (Table 3).

A weak positive correlation was found between the R_2* and areal BMD values (g/cm^2) (Fig. 3B). The R_2* and areal BMD values showed a significantly higher correlation in women than in men (r = 0.166 vs. 0.459 [reader 1]; r = 0.123 vs. 0.463 [reader 2]; p =0.048 [reader 1], 0.023 [reader 2]). For both readers, the highest correlation was found in postmenopausal women (Table 3).

Diagnostic Performance of the FF and R_2* for Predicting Osteopenia and Osteoporosis

The AUCs for the FF and R_2* for the prediction of osteopenic subjects were 0.651 and 0.664, respectively, for reader 1 and 0.647 and 0.654, respectively, for reader 2. Furthermore, the AUCs for normal and osteoporotic subject differentiation were 0.694 and 0.743, respectively, for reader 1 and 0.741 and 0.736, respectively, for reader 2. We found no significant differences in the diagnostic performance of the FF and R_2* for predicting osteopenia and osteoporosis. The ROC analysis showed that the combination of the FF and R_2* resulted in a higher AUC than that for the FF or R_2*alone for predicting osteopenia and osteoporosis. The $AUC_{osteopenia}$ and $AUC_{osteoporosis}$ were 0.716 and 0.758, respectively, for reader 1, and 0.720, and 0.763, respectively, for reader 2 (Table 4, Fig. 5).

In AUC comparisons, using the FF resulted in a higher AUC than using R_2* for predicting osteopenia and osteoporosis in older men; however, there were no significant differences ($AUC_{osteopenia}$, p = 0.015 [reader 1], 0.198 [reader 2]; $AUC_{osteoporosis}$, p = 0.620 [reader 1], 0.806 [reader 2]). In

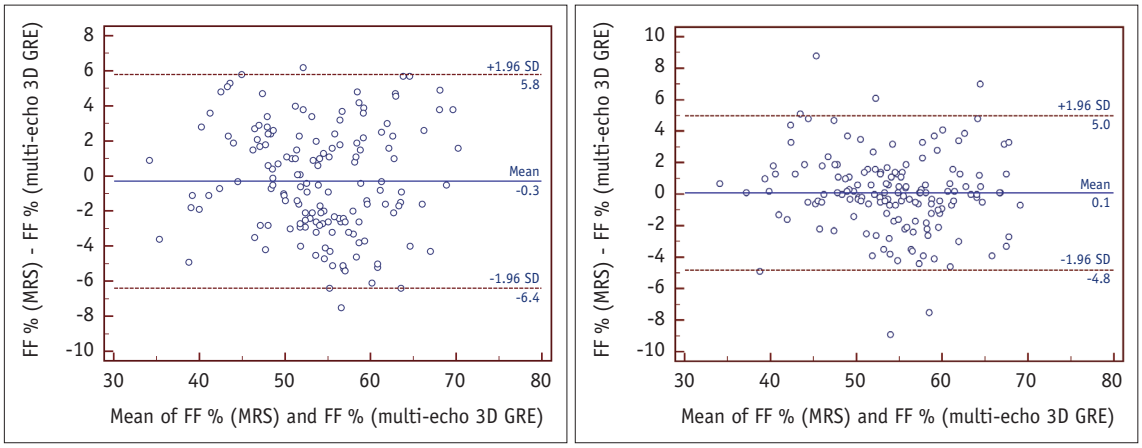

Fig. 4. Bland-Altman plots showing mean measurement bias with limits of agreement for FF derived from T_2*-corrected 6-echo Dixon VIBE imaging relative to that measured with MRS.

Mean measurement bias for reader 1 **(A)** was -0.3% (range, -6.4–5.8%), and mean measurement bias for reader 2 **(B)** was 0.1% (range, -4.8–5.0%). Mean bias is shown as solid line, and limits of agreement are shown as dashed lines.

Table 3. Correlations between BMD versus or R_2* in Each Group

Group	Reader 1				Reader 2			
	FF		R_2*		FF		R_2*	
	r	*P*	*r*	*P*	*r*	*P*	*r*	*P*
Male	-0.419	< 0.001	0.166	0.172	-0.427	< 0.001	0.123	0.315
Age < 50 years (n = 6)	-0.831	0.041	-0.158	0.765	-0.801	0.056	-0.127	0.811
Age ≥ 50 years (n = 63)	-0.370	0.003	0.207	0.103	-0.402	0.001	0.140	0.275
Female	-0.410	< 0.001	0.459	< 0.001	-0.442	< 0.001	0.463	< 0.001
Premenopausal (n = 7)	-0.623	0.135	0.036	0.940	-0.625	0.134	0.227	0.625
Postmenopausal (n = 77)	-0.403	< 0.001	0.626	< 0.001	-0.396	< 0.001	0.644	< 0.001
All	-0.411	< 0.001	0.358	< 0.001	-0.436	< 0.001	0.353	< 0.001

p values were calculated by Pearson's correlation analysis. FF = fat fraction

https://doi.org/10.3348/kjr.2018.0032

Korean Journal of Radiology
KJR

Table 4. Diagnostic Performance of FF, R_2*, and Combination of FF and R_2* for Predicting Osteopenia and Osteoporosis

Parameters	Normal vs. Osteopenia			Normal vs. Osteoporosis		
	FF	R_2*	FF + R_2*	FF	R_2*	FF + R_2*
Reader 1						
AUC	0.651 (0.561–0.727)	0.664 (0.568–0.734)	0.716 (0.636–0.793)	0.694 (0.609–0.776)	0.743 (0.653–0.819)	0.758 (0.669–0.832)
Sensitivity (%)	97.3 (85.8–99.9)	40.5 (24.8–57.9)	59.5 (42.1–75.2)	47.1 (23.0–77.0)	64.7 (38.3–85.8)	64.7 (38.3–85.8)
Specificity (%)	36.4 (26.9–46.6)	84.8 (76.2–91.3)	79.8 (70.5–87.2)	93.9 (87.3–97.7)	83.8 (75.1–90.5)	85.9 (77.4–92.0)
Cutoff value	> 49.6	≤ 14.9		> 62.5	≤ 15.0	
†p value	0.002	0.002	< 0.001	0.028	0.001	0.003
Reader 2						
AUC	0.647 (0.561–0.727)	0.654 (0.568–0.734)	0.720 (0.636–0.793)	0.741 (0.652–0.818)	0.736 (0.646–0.813)	0.763 (0.675–0.837)
Sensitivity (%)	89.2 (74.6–97.0)	45.9 (29.5–63.1)	56.8 (39.5–72.9)	58.8 (32.9–81.6)	70.6 (44.0–89.7)	70.6 (44.0–89.7)
Specificity (%)	41.4 (31.6–51.8)	79.8 (70.5–87.2)	77.8 (68.3–85.5)	90.9 (83.4–95.8)	67.7 (57.5–76.7)	81.8 (72.8–88.9)
Cutoff value	> 50.8	≤ 14.9		> 61.1	≤ 15.5	
†p value	0.003	0.003	< 0.001	0.002	0.001	< 0.001

Numbers in parentheses are lower and upper bounds of 95% CIs. †p value of AUC. AUC = area under curve, CI = confidence interval

postmenopausal women, the AUCs obtained using R_2* were higher than those obtained using the FF; however, significant differences were not observed ($AUC_{osteopenia}$, p = 0.260 [reader 1], 0.147 [reader 2]; $AUC_{osteoporosis}$, p = 0.257 [reader 1], 0.180 [reader 2]). The groups comprising younger men and premenopausal women had only one osteopenic and osteoporotic subject, which resulted in insufficient data for ROC curve analysis. In postmenopausal women, high sensitivity (90% for both readers) and excellent R_2* discriminatory capacity (AUC > 0.80 for both readers, p < 0.001) between normal individuals and patients with osteoporosis were observed. The FF combined with R_2* achieved a > 0.70 AUC value for predicting osteopenia and osteoporosis in older men and postmenopausal women. The AUCs for predicting osteopenia and osteoporosis in each group are summarized in Tables 5, 6 and Figures 6, 7.

DISCUSSION

Clinical interest in methods for accurately measuring vertebral marrow fat is increasing because vertebral marrow fat content is negatively correlated with BMD (8, 10-12, 27). Chemical shift-based water-fat separation techniques, such as iterative decomposition of water and fat with echo asymmetry and least-squares estimation and the modified Dixon technique, have a similar accuracy to MRS for fat quantification and are widely accepted as alternative techniques to MRS (15, 28). These techniques allow for more consistent water-fat separation by correcting for various confounding factors, such as main magnetic field inhomogeneity, multiple fat spectral peaks, and T_2*, T1 relaxation, and eddy current effects (13, 15, 28). The 3D T_2*-corrected 6-echo Dixon VIBE technique can obtain up to 32 echoes. This technique also supports multi-peak fat modeling and can quickly produce water- or fat-only images and R_2* maps using parallel acquisition and VIBE techniques (15, 17, 22). Compared with two-dimensional-acquisition water-fat imaging, the 3D T_2*-corrected 6-echo Dixon VIBE technique has certain advantages, including higher spatial resolution and wider coverage with a short scan time (15, 17, 22). Our study used the 3D T_2*-corrected 6-echo Dixon VIBE technique and simultaneously performed T_1 bias and T_2* corrections to more accurately quantify marrow fat.

Our results showed that T_2*-corrected 6-echo Dixon VIBE imaging allows for accurate quantification of vertebral marrow fat and is comparable to MRS. We found sex-, age-, and menopause-related differences in associations between the FF, R_2*, and BMD. These results indicate that various conclusions can be reached depending on which group is included. We also investigated whether

 https://doi.org/10.3348/kjr.2018.0032

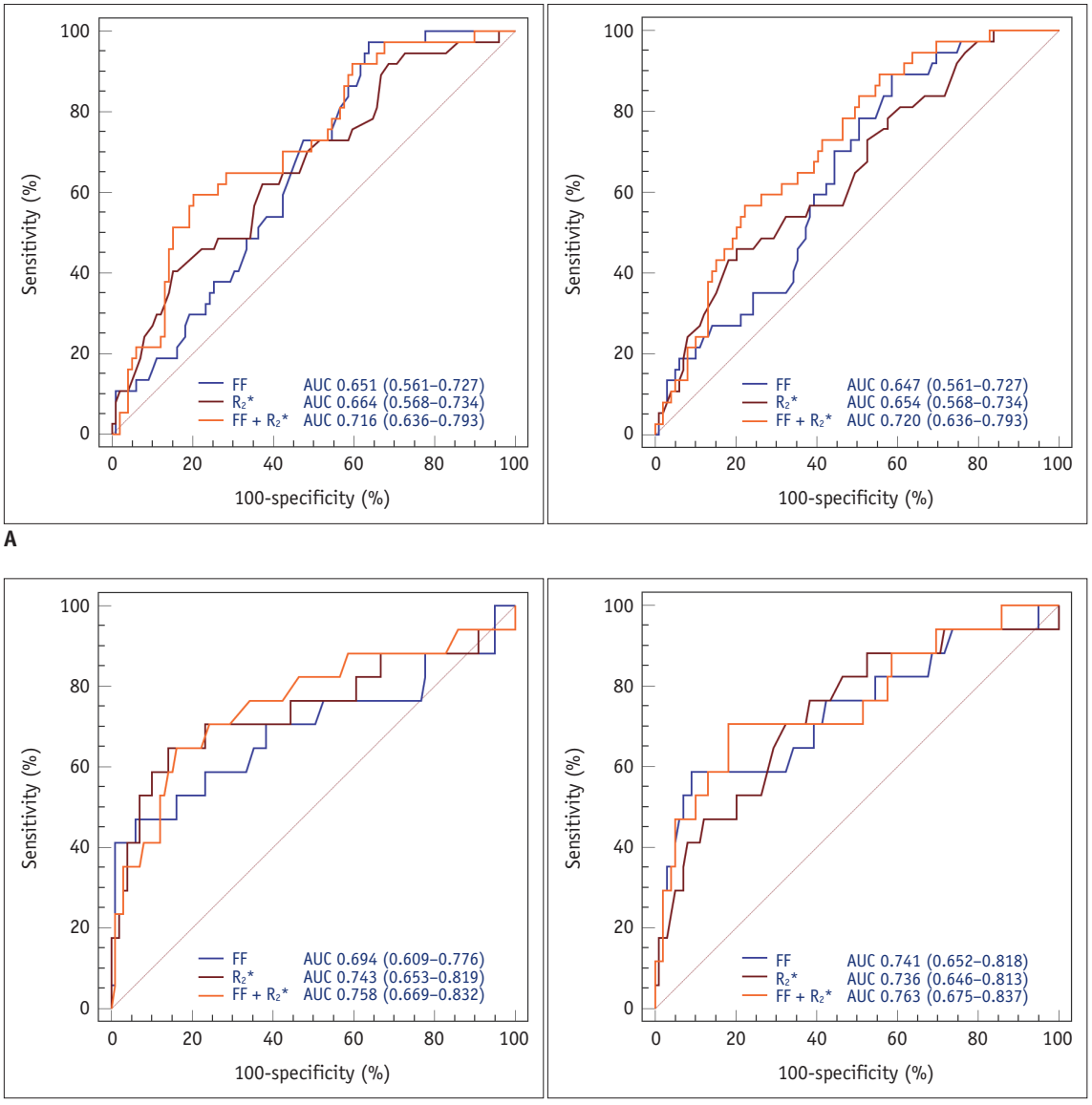

Fig. 5. Graphs showing ROC curves of readers 1 and 2 for predicting osteopenia (reader 1, A-left; reader 2, A-right) and osteoporosis (reader 1, B-left; reader 2, B-right) using FF, R_2*, or combination of FF and R_2*. ROC analysis demonstrated that combination of FF and R_2* improved diagnostic performance for predicting osteopenia and osteoporosis for both readers. AUC = area under curve, ROC = receiver operating characteristic

these parameters can be used as biomarkers for predicting osteopenia and osteoporosis. The combination of the FF and R_2* showed fair to excellent diagnostic performance for the detection of osteopenia and osteoporosis. However, compared with the FF or R_2* alone, the combination of the FF and R_2* showed only a minor or no improvement in performance. This finding might be due to differences in individual bone marrow composition and various microenvironmental conditions related to medical history or physical activity. Although the difference did not reach significance, it showed optimal specificity and sensitivity in postmenopausal women.

Our data indicate a moderate inverse correlation between the FF and BMD in all of the patients, consistent with the results of previous studies (27-29). However, we found that the correlation was weaker in older men and postmenopausal women. Physiological changes related to aging or menopause might be considered potential causes of the relatively weak correlation between the FF and BMD in these subgroups. For example, red marrow reconversion can increase with age due to the increased risk of cancer, infection, trauma, or other stress that occurs with aging.

https://doi.org/10.3348/kjr.2018.0032

Korean Journal of Radiology
KJR

Table 5. Diagnostic Performance of FF, R_2*, and Combination of FF and R_2* for Predicting Osteopenia in Each Group

Parameters	Males (Age ≥ 50 Years)				Females (Postmenopausal)			
	Sensitivity (%)	Specificity (%)	AUC	$P^{\dagger}$	Sensitivity (%)	Specificity (%)	AUC	$P^{\dagger}$
FF								
Reader 1	100.0	52.3	0.779 (0.651–0.877)	0.001	96.8	25.0	0.604 (0.477–0.721)	0.135
Reader 2	100.0	46.2	0.768 (0.638–0.868)	0.005	96.8	27.8	0.620 (0.493–0.736)	0.083
R_2*								
Reader 1	100.0	26.9	0.518 (0.383–0.651)	0.897	74.2	61.1	0.699 (0.575–0.805)	0.003
Reader 2	100.0	32.8	0.526 (0.390–0.658)	0.856	74.2	72.2	0.735 (0.613–0.835)	< 0.001
FF + R_2*								
Reader 1	100.0	59.6	0.782 (0.654–0.880)	< 0.001	67.7	72.2	0.702 (0.577–0.807)	0.002
Reader 2	100.0	46.2	0.766 (0.636–0.867)	0.005	77.4	66.7	0.736 (0.614–0.836)	< 0.001

Younger males and premenopausal females included only one osteopenic subject, resulting in insufficient data for ROC curve analysis. Numbers in parentheses are lower and upper bounds of 95% CIs. $^{\dagger}p$ value of AUC. ROC = receiver operating characteristic

Table 6. AUC of FF, R_2*, and Combination of FF and R_2* for Predicting Osteoporosis in Each Group

Parameters	Males (Age ≥ 50 Years)				Females (Postmenopausal)			
	Sensitivity (%)	Specificity (%)	AUC	$P^{\dagger}$	Sensitivity (%)	Specificity (%)	AUC	$P^{\dagger}$
FF								
Reader 1	75.0	94.3	0.726 (0.592–0.836)	0.326	40.0	100.0	0.689 (0.535–0.817)	0.113
Reader 2	75.0	98.1	0.762 (0.630–0.865)	0.234	50.0	88.9	0.667 (0.512–0.799)	0.158
R_2*								
Reader 1	100.0	35.8	0.651 (0.513–0.772)	0.200	90.0	86.1	0.868 (0.736–0.950)	< 0.001
Reader 2	100.0	47.2	0.698 (0.562–0.813)	0.038	90.0	83.3	0.860 (0.726–0.944)	< 0.001
FF + R_2*								
Reader 1	75.0	92.5	0.717 (0.582–0.818)	0.341	90.0	83.3	0.872 (0.741–0.952)	< 0.001
Reader 2	75.0	96.2	0.778 (0.649–0.878)	0.172	90.0	86.1	0.867 (0.734–0.949)	< 0.001

Younger males and premenopausal females included only one osteoporotic subject, resulting in insufficient data for ROC curve analysis. Numbers in parentheses are lower and upper bounds of 95% CIs. $^{\dagger}p$ value of AUC.

Moreover, the prevalence of Modic changes increases with age (30, 31). Modic type 1 and 2 changes are uncommon in patients before 50 years of age, but they increase after the age of 50 years with type 2 changes being more common. Modic type 1 and 2 changes are most frequently encountered at L4–5 and L5–S1, and L4–5 is the most common site of such changes (30, 31). The mean ages of the older men and postmenopausal women were significantly higher than those of the other groups combined. Additionally, relative estrogen deficiency accelerates vertebral endplate and disc degeneration. In fact, severe lumbar disc degeneration tends to be more common in postmenopausal women than in elderly men (32). Recent studies have demonstrated that Modic type 2 change is primarily associated with severe disc degeneration (33, 34). Compared with Modic type 2 changes, which are associated with fatty degeneration,

 https://doi.org/10.3348/kjr.2018.0032

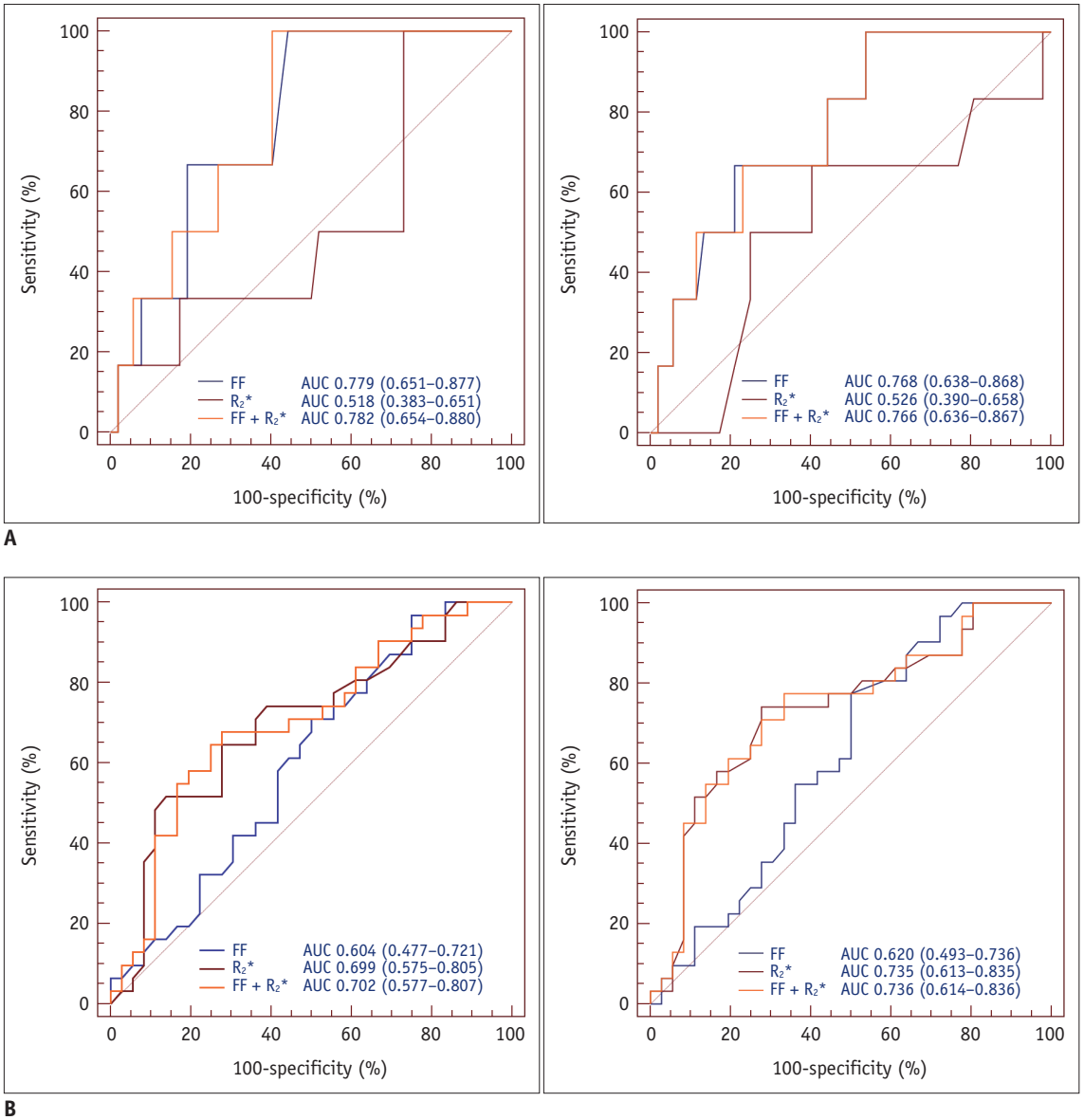

Fig. 6. ROC analysis of FF, R_2*, and combination of FF and R_2* for predicting osteopenia (reader 1, A-left; reader 2, A-right) and osteoporosis (reader 1, B-left; reader 2, B-right) in older men. ROC analysis demonstrated that AUCs for FF were higher than those for R_2* for both readers. However, ROC curve showed only minor improvements in diagnostic performance for predicting osteopenia and osteoporosis.

Modic type 1 changes are associated with increased vascularity and marrow edema (30, 31). However, Modic type 1 changes have been associated with higher FF values than those in normal marrow. We drew ROIs at least 2 mm from the endplate to exclude the cortical bone. Moreover, focal fat deposits were excluded. However, Modic changes were observed in both sides of the endplates as well as in large confluent areas of the vertebral body (30). The various degrees of Modic changes included in the ROIs are assumed to affect the vertebral marrow composition.

MRS is currently used as the non-invasive gold standard for the clinical assessment of vertebral marrow fat content (5-10). MRS presents no risk of exposure to ionizing radiation and adequately reflected marrow fat as demonstrated by a histopathological study (35). However, MRS has certain limitations, such as the inability to cover an entire vertebral marrow segment with a single voxel and certain technical challenges (14, 16, 28). Moreover, performing fat measurements is impracticable because MRS requires the creation of a more homogeneous B_0 field with shimming. In contrast to previous studies (16, 36), for the FF measurements, we attempted to draw ROIs including as much bone marrow as possible, while excluding the vertebral endplate and cortical bone. We confirmed excellent

https://doi.org/10.3348/kjr.2018.0032

Korean Journal of Radiology
KJR

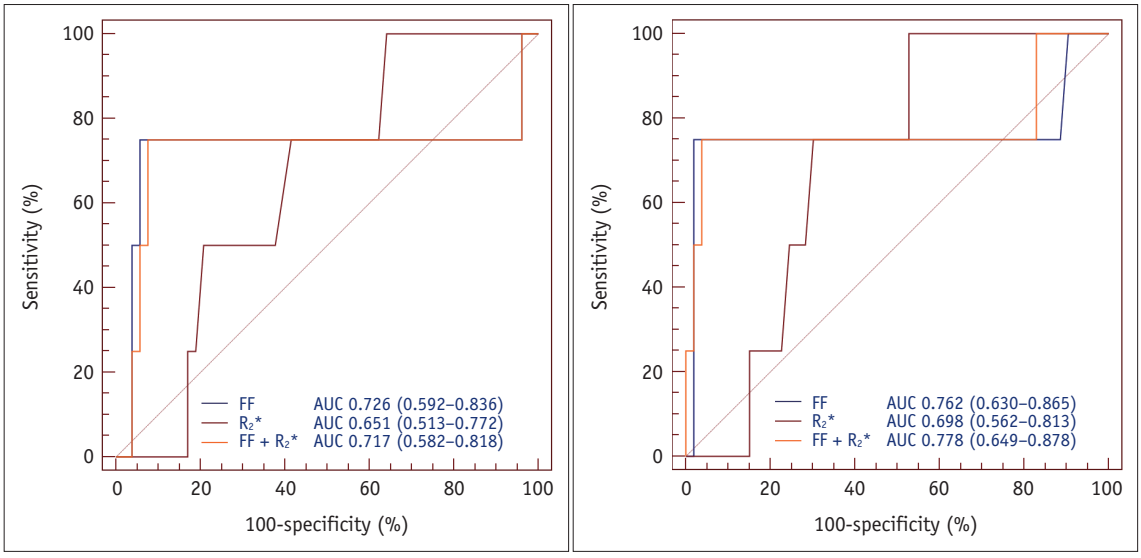

Fig. 7. ROC analysis of FF, R_2*, and combination of FF and R_2* for predicting osteopenia (reader 1, A-left; reader 2, A-right) and osteoporosis (reader 1, B-left; reader 2, B-right) in postmenopausal women. ROC analysis demonstrated that AUCs for R_2* were excellent for both readers. However, there was no significant difference in AUCs between FF, R_2*, and combination of FF and R_2*.

consistency between T_2*-corrected 6-echo Dixon VIBE imaging and MRS measurements. Therefore, T_2*-corrected 6-echo Dixon VIBE imaging is expected to enable accurate quantification of vertebral marrow fat in a short scan time as well as provide both quantitative and spatially-resolved information on vertebral marrow fat. Although our study only measured a single vertebra, the T_2*-corrected 6-echo Dixon VIBE technique can collect data for multiple vertebral levels in one acquisition.

T_2*-corrected 6-echo Dixon VIBE imaging has the additional advantage of simultaneously obtaining the R_2* value with fat quantification (21). Previous studies showed that multi-peak modeling of fat signals yielded better accuracy than single-peak fat modeling, which induced an underestimation of the fat signals (20, 21). We also performed multi-peak fat modeling. We found a positive correlation between the R_2* and areal BMD values, which is consistent with the results of a previous study, and both studies used R_2* with multi-peak fat correction (22). The R_2* map is a byproduct of T_2*-corrected fat quantification and equivalent to $1/T_2$* (20, 21). In patients with osteoporosis, T_2* decay is assumed to be delayed because of trabecular bone loss, which will decrease R_2* (22). We found that there was a significant difference between men

https://doi.org/10.3348/kjr.2018.0032

and women in the relationship of R_2* with areal BMD. It is well known that quantitatively measured serum ferritin is a reliable indicator of bone marrow iron stores (37). A recent study showed a significant correlation between serum ferritin and BMD in women ≥ 45 years of age (38). This finding may be explained by the rapid loss of estrogen in these women. In agreement with that study, the highest correlation coefficient between R_2* and BMD was observed in postmenopausal women in the present study.

In a previous study, the question of whether the FF or R_2* alone could be used as a marker to assess osteoporosis was raised (22). Moreover, the FF and R_2* are not reliable for osteopenia assessment. We found that the FF and R_2*showed poor to fair performance in all subjects. Additionally, ROC curve analysis showed that the AUC of the combination of the FF and R_2* was higher than those of the FF or R_2* alone. We focused on differences in diagnostic performance between the FF and R_2* according to sex and menopause status. The AUC of R_2* was higher than that of the FF in postmenopausal women and showed good discriminatory performance in predicting osteoporosis. The FF showed good performance in older men, but poor performance in postmenopausal women. The combination of the FF and R_2* showed good performance (AUC > 0.7) in older men and postmenopausal women; however, it only showed minor or no improvement in performance compared with the FF and R_2* alone. Vertebral marrow fat increases sharply in postmenopausal women (39), and this disproportionate increase in marrow fat consequently contributes to the loss of trabecular bone (40). A possible explanation for our finding may be that the loss of trabecular bone eventually led to a reduction in R_2*, which led to better diagnostic performance.

Our study has certain limitations. First, the sample sizes of the younger men and premenopausal women were smaller than those of the other two subgroups. Second, the MRS data were used as the reference standards for fat content quantification. True marrow fat content can only be assessed via bone biopsy; however, this was practically impossible. Third, we only used DXA to assess bone mineralization, even though bone strength is determined by various factors, including bone mass and microarchitecture; however, DXA only reflects bone mass (41). Fourth, all subjects were patients who reported low back pain. Thus, the possibility of bias cannot be ruled out. Fifth, we did not compare the diagnostic efficacy between the uncorrected FF and T_2*-corrected FF. Finally, patients with severe osteophytes or degenerative changes were excluded because of the possibility of distorted BMD results, which potentially limits the applicability of the study outcomes to normal vertebrae.

In summary, T_2*-corrected 6-echo Dixon VIBE imaging is feasible and can be used as an alternative technique for estimating the vertebral marrow FF. In addition, the R_2* value can be obtained as a byproduct of T_2* correction. The FF and R_2* values obtained using T_2*-corrected 6-echo Dixon VIBE imaging could potentially serve as predictors of osteopenia and osteoporosis. R_2* might be useful for predicting osteoporosis, especially in postmenopausal women.

Conflicts of Interest

The authors have no potential conflicts of interest to disclose.

ORCID iDs

Sun Joo Lee
https://orcid.org/0000-0001-6210-9720
Donghyun Kim
https://orcid.org/0000-0002-3429-7557

REFERENCES

1. Consensus Development Conference: diagnosis, prophylaxis and treatment of osteoporosis. *Am J Med* 1993;94:646-650
2. Lane NE. Epidemiology, etiology, and diagnosis of osteoporosis. *Amer J Obstet Gynecol* 2006;194(2 Suppl):S3-S11
3. Kanis JA, McCloskey EV, Johansson H, Oden A, Melton LJ 3rd, Khaltaev N. A reference standard for the description of osteoporosis. *Bone* 2008;42:467-475
4. Rosen CJ, Bouxsein ML. Mechanisms of disease: is osteoporosis the obesity of bone? *Nat Clin Pract Rheumatol* 2006;2:35-43
5. Bredella MA, Daley SM, Kalra MK, Brown JK, Miller KK, Torriani M. Marrow adipose tissue quantification of the lumbar spine by using dual-energy CT and single-voxel (1)H-MR spectroscopy: a feasibility study. *Radiology* 2015;277:230-235
6. Gee CS, Nguyen JT, Marquez CJ, Heunis J, Lai A, Wyatt C, et al. Validation of bone marrow fat quantification in the presence of trabecular bone using MRI. *J Magn Reson Imaging* 2015;42:539-544
7. Karampinos DC, Melkus G, Baum T, Bauer JS, Rummeny EJ, Krug R. Bone marrow fat quantification in the presence of trabecular bone: initial comparison between water-fat imaging and single-voxel MRS. *Magn Reson Med* 2014;71:1158-1165
8. Li X, Kuo D, Schafer AL, Porzig A, Link TM, Black D, et al. Quantification of vertebral bone marrow fat content using 3

https://doi.org/10.3348/kjr.2018.0032

tesla MR spectroscopy: reproducibility, vertebral variation, and applications in osteoporosis. *J Magn Reson Imaging* 2011;33:974-979
9. Singhal V, Miller KK, Torriani M, Bredella MA. Short- and long-term reproducibility of marrow adipose tissue quantification by 1H-MR spectroscopy. *Skeletal Radiol* 2016;45:221-225
10. Yeung DKW, Griffith JF, Antonio GE, Lee FKH, Woo J, Leung PC. Osteoporosis is associated with increased marrow fat content and decreased marrow fat unsaturation: a proton MR spectroscopy study. *J Magn Reson Imaging* 2005;22:279-285
11. Griffith JF, Yeung DK, Antonio GE, Lee FK, Hong AW, Wong SY, et al. Vertebral bone mineral density, marrow perfusion, and fat content in healthy men and men with osteoporosis: dynamic contrast-enhanced MR imaging and MR spectroscopy. *Radiology* 2005;236:945-951
12. Griffith JF, Yeung DK, Antonio GE, Wong SY, Kwok TC, Woo J, et al. Vertebral marrow fat content and diffusion and perfusion indexes in women with varying bone density: MR evaluation. *Radiology* 2006;241:831-838
13. Shen W, Gong X, Weiss J, Jin Y. Comparison among T1-weighted magnetic resonance imaging, modified Dixon method, and magnetic resonance spectroscopy in measuring bone marrow fat. *J Obes* 2013;2013:298675
14. Li G, Xu Z, Gu H, Li X, Yuan W, Chang S, et al. Comparison of chemical shift-encoded water-fat MRI and MR spectroscopy in quantification of marrow fat in postmenopausal females. *J Magn Reson Imaging* 2017;45:66-73
15. Li GW, Xu Z, Chen QW, Tian YN, Wang XY, Zhou L, et al. Quantitative evaluation of vertebral marrow adipose tissue in postmenopausal female using MRI chemical shift-based water-fat separation. *Clin Radiol* 2014;69:254-262
16. Yoo HJ, Hong SH, Kim DH, Choi JY, Chae HD, Jeong BM, et al. Measurement of fat content in vertebral marrow using a modified dixon sequence to differentiate benign from malignant processes. *J Magn Reson Imaging* 2017;45:1534-1544
17. Le Ster C, Gambarota G, Lasbleiz J, Guillin R, Decaux O, Saint-Jalmes H. Breath-hold MR measurements of fat fraction, T1, and T2* of water and fat in vertebral bone marrow. *J Magn Reson Imaging* 2016;44:549-555
18. Yu H, Shimakawa A, McKenzie CA, Brodsky E, Brittain JH, Reeder SB. Multiecho water-fat separation and simultaneous R2* estimation with multifrequency fat spectrum modeling. *Magn Reson Med* 2008;60:1122-1134
19. Fischer MA, Nanz D, Shimakawa A, Schirmer T, Guggenberger R, Chhabra A, et al. Quantification of muscle fat in patients with low back pain: comparison of multi-echo MR imaging with single-voxel MR spectroscopy. *Radiology* 2013;266:555-563
20. Yoo YH, Kim HS, Lee YH, Yoon CS, Paek MY, Yoo H, et al. Comparison of multi-echo Dixon methods with volume interpolated breath-hold gradient echo magnetic resonance imaging in fat-signal fraction quantification of paravertebral muscle. *Korean J Radiol* 2015;16:1086-1095
21. Kühn JP, Hernando D, Muñoz del Rio A, Evert M, Kannengiessre S, Völzke H, et al. Effect of multipeak spectral modeling of fat for liver iron and fat quantification: correlation of biopsy with MR imaging results. *Radiology* 2012;265:133-142
22. Kühn JP, Hernando D, Meffert PJ, Reeder S, Hosten N, Laqua R, et al. Proton-density fat fraction and simultaneous R2* estimation as an MRI tool for assessment of osteoporosis. *Eur Radiol* 2013;23:3432-3439
23. Koo TK, Li MY. A guideline of selecting and reporting intraclass correlation coefficients for reliability research. *J Chiropr Med* 2016;15:155-163
24. Lin LI. A concordance correlation coefficient to evaluate reproducibility. *Biometrics* 1989;45:255-268
25. Dancey CP, Reidy J. *Statistics without maths for psychology*, 5th ed. New York, NY: Pearson Prentice Hall, 2011:175-176
26. McCallum RS. *Handbook of Nonverbal Assessment*, 2nd ed. Cham: Springer, 2017:182
27. Schwartz AV, Sigurdsson S, Hue TF, Lang TF, Harris TB, Rosen CJ, et al. Vertebral bone marrow fat associated with lower trabecular BMD and prevalent vertebral fracture in older adults. *J Clin Endocrinol Metab* 2013;98:2294-2300
28. Ergen FB, Gulal G, Yildiz AE, Celik A, Karakaya J, Aydingoz U. Fat fraction estimation of the vertebrae in females using the T2*-IDEAL technique in detection of reduced bone mineralization level: comparison with bone mineral densitometry. *J Comput Assist Tomogr* 2014;38:320-324
29. Shen W, Scherzer R, Gantz M, Chen J, Punyanitya M, Lewis CE, et al. Relationship between MRI-measured bone marrow adipose tissue and hip and spine bone mineral density in African-American and Caucasian participants: the CARDIA study. *J Clin Endocrinol Metab* 2012;97:1337-1346
30. Chung CB, Vande Berg BC, Tavernier T, Cotton A, Laredo JD, Vallee C, et al. End plate marrow changes in the asymptomatic lumbosacral spine: frequency, distribution and correlation with age and degenerative changes. *Skeletal Radiol* 2004;33:399-404
31. Karchevsky M, Schweitzer ME, Carrino JA, Zoga A, Montgomery D, Parker L. Reactive endplate marrow changes: a systematic morphologic and epidemiologic evaluation. *Skeletal Radiol* 2005;34:125-129
32. Wang YX, Griffith JF. Effect of menopause on lumbar disk degeneration: potential etiology. *Radiology* 2010;257:318-320
33. Teichtahl AJ, Urquhart DM, Wang Y, Wluka AE, O'Sullivan R, Jones G, et al. Lumbar disc degeneration is associated with modic change and high paraspinal fat content - a 3.0T magnetic resonance imaging study. *BMC Musculoskelet Disord* 2016;17:439
34. Teichtahl AJ, Urquhart DM, Wang Y, Wluka AE, O'Sullivan R, Jones G, et al. Modic changes in the lumbar spine and their association with body composition, fat distribution and intervertebral disc height - a 3.0 T-MRI study. *BMC Musculoskelet Disord* 2016;17:92
35. Li GW, Tang GY, Liu Y, Tang RB, Peng YF, Li W. MR spectroscopy and micro-CT in evaluation of osteoporosis model in rabbits: comparison with histopathology. *Eur Radiol* 2012;22:923-929
36. Kim DH, Yoo HJ, Hong SH, Choi JY, Chae HD, Chung BM.

https://doi.org/10.3348/kjr.2018.0032

Differentiation of acute osteoporotic and malignant vertebral fractures by quantification of fat fraction with a Dixon MRI sequence. *AJR Am J Roentgenol* 2017;209:1331-1339
37. Rocha LA, Barreto DV, Barreto FC, Dias CB, Moysés R, Silva MR, et al. Serum ferritin level remains a reliable marker of bone marrow iron stores evaluated by histomorphometry in hemodialysis patients. *Clin J Am Soc Nephrol* 2009;4:105-109
38. Kim BJ, Lee SH, Koh JM, Kim GS. The association between higher serum ferritin level and lower bone mineral density is prominent in women ≥ 45 years of age (KNHANES 2008-2010). *Osteoporos Int* 2013;24:2627-2637
39. Griffith JF, Yeung DK, Ma HT, Leung JC, Kwok TC, Leung PC. Bone marrow fat content in the elderly: a reversal of sex difference seen in younger subjects. *J Magn Reson Imaging* 2012;36:225-230
40. Roldan-Valadez E, Piña-Jimenez C, Favila R, Rios C. Gender and age groups interactions in the quantification of bone marrow fat content in lumbar spine using 3T MR spectroscopy: a multivariate analysis of covariance (Mancova). *Eur J Radiol* 2013;82:e697-e702
41. Griffith JF, Genant HK. Bone mass and architecture determination: state of the art. *Best Pract Res Clin Endocrinol Metab* 2008;22:737-764

https://doi.org/10.3348/kjr.2018.0032